Active nonlinear spectroscopy of biexcitons in semiconductors: Propagation effects and Fano interferences

A. Maruani and D. S. Chemla
Centre National d'Etudes des Télécommunications, 92220 Bagneux, France*
(Received 27 May 1980)

Four-wave degenerate-frequency mixing is used to study experimentally and theoretically the Γ_1 biexciton in CuCl and CdS. Propagation and polarization effects, which are particularly important in the case of CdS, are evidenced; giant oscillator strengths and autoionizing characters are also revealed. A formalism is sketched, which describes, for a coherent anti-Stokes Raman scattering-type experiment, the most general third-order susceptibility tensor in a solid where a three-nearly-equidistant-level system is distinguished amidst a large number of other, nonresonant, levels and where there is one two-photon-resonant autoionizing state. The propagation analysis accounts accurately on one side for the large shifts between the maxima of the spectra and the energetic position of the resonances, and on the other side for the severe nonlinearities and the highly structured profile of the observed line shapes. Thus, a very satisfactory agreement between experiment and theory is obtained and a number of biexciton parameters, including Fano's q parameter, is determined.

INTRODUCTION

Nonlinear active phenomena in semiconductors are the subject of intense and fruitful studies.[1] Their use is particularly convenient if one investigates the energy levels around and above the fundamental energy gaps, where linear absorptions are very high, and then conventional optical studies limited to small regions near the surface of the samples. The reasons for that growing popularity include: (a) The selection rules can be made different from those of one-photon transitions, or complementary to them. (b) One deals with coherent processes allowing us to discriminate between the states involved in the phenomena, and to deal with laserlike signals. (c) Frequency transposition, so that a highly absorbing region of the crystal can be studied in the transparency region. A very popular configuration is the Coherent anti-stokes Raman scattering[2] (CARS) where a signal at frequency $\omega_3 = 2\omega_1 - \omega_2$ is created through the mixing of two beams at frequencies ω_1 and ω_2.

The wave vector of the signal is, with standard notations, $\vec{k}_3 = 2\vec{k}_1 - \vec{k}_2$; in other terms, the efficiency of the process is maximum when the phase mismatch $\Delta\vec{k}\cdot\vec{l} = (2\vec{k}_1 - \vec{k}_2 - \vec{k}_3)\cdot\vec{l}$ is null, $\vec{l}$ being the sample-thickness vector. That condition may be very difficult or impossible to achieve in the energy regions we are interested in ($h\nu \approx E_g$) and that is due to the strong dispersion of the refractive index n related to the large absorption coefficient α ($\alpha \sim 10^2$–10^3 cm^{-1}) in the tail of an electronic resonance.

That difficulty is overcome if one works in the energy-degenerate configuration where all beams have the same frequency, but different wave vectors.[3(a)] In that case, the process is symbolized by the two conservation equations

$$\omega = \omega + \omega - \omega ,$$
$$\vec{k}_s = 2\vec{k}_p - \vec{k}_t ,$$

where the exciting beams are labeled pump and test beam, respectively, with wave vectors $\vec{k}_p$ and $\vec{k}_t$, giving rise to the signal with wave vector $\vec{k}_s$. In Fig. 1 the principle of the experiment as well as the corresponding energy levels and $\vec{k}$ vector diagrams are schematized. Note that the exciting beams originate from the same laser.

Since the same refractive index holds for all beams, the phase-matching criterion reduces to $\measuredangle(k_p, k_t)$ as small as possible compatible with spatial discrimination. For a typical situation, that angle is smaller than 2° outside the sample, so that the ratio ϵ = sample thickness: coherence length $= l/l_c$ is always much smaller than unity and the efficiency of the process, as given by $\eta = \sin^2 c(\Delta\vec{k}\cdot\vec{l}/2)$ is, for typical situations and neglecting one- and two-photon absorption, 90–95% of its maximum value. Introduction of the absorption should not alter significantly the trends of this result.

We have applied the method sketched above to study the biexciton level in semiconductors. We first consider the simpler case of CuCl and then the more involved one of CdS. The main reason for the choice of our method is that, prior to our investigations, no method based on coherent scattering was applied to the study of biexcitons and, as shown below, one can forecast that active nonlinear spectroscopy is well suited to probing these levels.

A very great number of papers exists concerning the biexciton in semiconductors, and its existence

 © 1981 The American Physical Society

has been reported for many of them. The reader may refer to the two reviews of Hanamura and Haug[4] and Lévy *et al.*[5] Concerning CuCl, one can mention, e.g., time-resolved luminescence,[6(a)] light mixing,[6(b)] absorption, emission, excitation spectra,[6(c)] stimulated emission,[6(d)] polarization luminescence,[6(e)] and hyper-Raman scattering.[6(f)] Concerning CdS, one can mention optical gain,[7(a)] induced absorption,[7(b)] and resonant hyper-Raman scattering,[7(c)] two-photon absorption (TPA),[7(d)] photoluminescence,[7(e)] and luminescence assisted TPA.[7(f)] The references in Refs. 6 and 7 are a small part of the very abundant literature on the respective topics.

All those works agree concerning the following values for the formation energies of the molecule: $W_{X_2} = 5.10$ and 6.37 eV, respectively, for CdS and CuCl; the damping parameter is not always indicated since its determination is often submitted to a model in which hypotheses have to be made on the relaxation mechanism. The precise determination of the exciton-biexciton oscillator strength

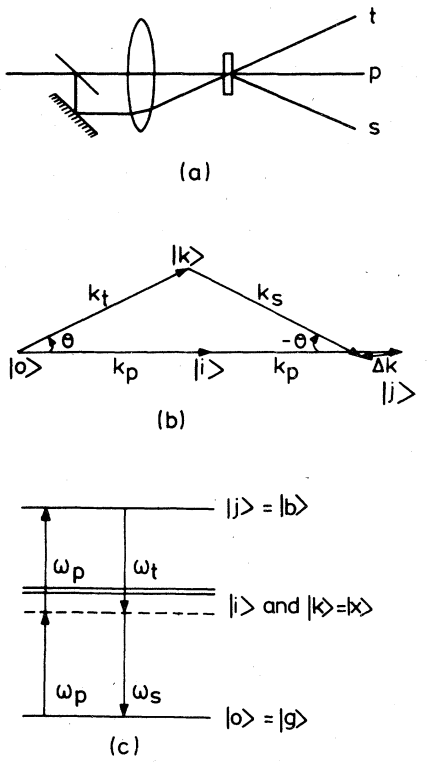

FIG. 1. Principles of the method of forward degenerate optical mixing. (a) Principle of the experimental setup. (b) Geometrical construction for the phase-matching condition, legitimating the symmetry of (a) ($\Delta\vec{k} \ll k_p$, k_t, k_s) $|g\rangle$ = ground state, $|x\rangle$ = exciton states, $|b\rangle$ = biexciton state. All energies are identical. (c) Representation of the states involved in (b).

(or absorption coefficient) is also a quantity very hard to measure accurately or compute. These difficulties find their origin in the fact that in most of those experiments, an excitonic molecule has to be actually excited, and to decay in the sample to allow an experimental determination of its parameters. We investigate here a method where at no moment is an excitonic molecule detected from its *decay* through luminescence or hyper-Raman scattering.

By contrast, our method is sensitive to the *virtual excitation* mechanism of the excitonic molecule, through the resonance of a nonlinear polarization. Then, no actual change of the populations (diagonal elements of the density matrix) occurs and our signals result from the resonance of only coherent states, those which are described by the off-diagonal terms of the density matrix. The signal production is governed by the third-order susceptibility tensor $\chi^{(3)}(-\omega;\omega,\omega,-\omega)$ through the relation $P_s = \epsilon_0 \chi^{(3)} \vdots E_p E_p E_t^*$ where P_s is the induced polarization and E the electric fields. It is expected to be maximum around $\hbar\omega = \frac{1}{2} W_{x2}$; then $\hbar\omega$ is close to the formation energy of the exciton and what is actually observed is a multiple resonance which is so efficient that multiple scatterings up to the fourth order are easily evidenced.[3(b)] This paper is devoted to the study of the first-order scattering. As will be shown later, the gain is given by the modulus of $\chi^{(3)}$, whereas two-photon absorption is given by its imaginary part, which is resonant for the same energy $\frac{1}{2} W_{x_2}$. Then one has to account precisely for these competing phenomena.

Section I is devoted to the theoretical analysis of the process, i.e., the study of the propagation effects and the study of $\chi^{(3)}$. We shall recall there exact analytical solutions for the beam intensities and discuss the expressions for $\chi^{(3)}$ needed to describe third-order processes in crystals. Section II is devoted to the study of the experimental procedure and the experimental results: We shall stress the peculiarities of the resonance line shapes and the nonlinearities of the phenomena. Section III will discuss the problems raised by the experimental results in terms of the two-photon autoionizing description for the biexciton state,[8] and will present the results and the discussion of our analysis, as well as some indications on further theoretical and experimental results.

I. THEORY

A. Propagation effects in forward-degenerate four-wave mixing (FDFWM)

In coherent optical scatterings, propagation ef-

fects are very important especially for multiresonant phenomena, as is our case. They need to be precisely accounted for if one wishes to extract physical parameters from the experimental data. An exhaustive discussion of the propagation effects associated with FDFWM has been given by one of the authors[9]; in this section, we briefly recall the results relevant for our experiment. The procedure is usual in nonlinear optics[10]: One collects the nonlinear polarization contributions with proper frequencies and wave vectors, and then introduces them as source terms in the corresponding Maxwell equations. As indicated in the Introduction, the mixing can safely be assumed as phase matched. In the slowly varying envelope approximation[11] (the validity of this approximation has been checked *a posteriori* in the case of the two compounds we have investigated: for instance for CuCl at resonance where the conditions are the most severe), one has

$$\left|\frac{\partial^2 E}{\partial z^2}\right| \simeq 10^{-3}\left|\frac{k\partial E}{\partial z}\right| .$$

One obtains the set of three complex coupled equations:

$$\frac{dE_p}{dz}+\frac{\alpha_p}{2}E_p - i\kappa\left(\frac{|E_p|^2}{2}+|E_t|^2+|E_s|^2\right)E_p = i\kappa E_p^* E_t E_s$$

$$\frac{dE_i}{dz}+\frac{\alpha_i}{2}E_i - i\kappa\left(\frac{|E_i|^2}{2}+|E_p|^2+|E_j|^2\right)E_i = \frac{i\kappa}{2}E_p^2 E_j^* \quad (i\neq j)$$

where $(i,j)=(t,s)$, the α are the linear absorption coefficients, and $\kappa=\omega\chi^{(3)}(\epsilon_0 n^2 c^2)^{-1}$ is the nonlinear coupling coefficient. The terms in parentheses describe a nonlinear change of the absorption, associated with $\mathrm{Im}(\kappa)=\kappa_2$ and a nonlinear change of refractive index, associated with $\mathrm{Re}(\kappa)=\kappa_1$. Those changes are induced by the field itself, or can be introduced by the two other fields; within that latter case is an enhancement of two of the effects, as discussed in Ref. 9. The right-hand-side terms describe either the depletion of the pump or the gain in the two other fields. Their quantum interpretation is that, for each microscopic process, two photons on the pump beam are annihilated and one test and one signal photon are created. That explains the factor 2 appearing in the coupling constant of the pump-depletion term as compared with that of the signal and test nonlinear gain.

For the most general configuration, one has to solve numerically the system of six coupled nonlinear real equations. That is the procedure we have used to proceed to the data analysis without any further approximation. Now, it is possible to find an analytical solution which displays clearly the physical meaning of the observed spectra, and which is operational as far as the initial values of the test and pump beam intensities, $I_t(0)$ and $I_p(0)$, are such that the ratio $I_t(0)/I_p(0)$ is lower than 0.5. Experimentally, our maximum value for that ratio is $\frac{1}{3}$ and most of the spectra were recorded with $10^{-2}\leq I_t(0)/I_p(0)\leq 10^{-1}$. Then, the signal intensity also remains small as compared to the pump one and the following assumptions are valid:

(i) The pump attenuation is due essentially to the linear absorption and to the self-TPA; the pump depletions related to induced TPA and nonlinear gain are negligible.

(ii) The phase shifts associated with the Kerr effect are essentially due to the pump beam.

(iii) The signal and test attenuations are the linear absorption and the pump-induced TPA.

Consequently, the coupled-equation system is written:

$$\frac{dE_p}{dz}+\left(\frac{\alpha_p}{2}-\frac{i\kappa}{2}|E_p|^2\right)E_p=0 ,$$

$$\frac{dE_t}{dz}+\left(\frac{\alpha}{2}-i\kappa|E_p|^2\right)E_t=\frac{i\kappa}{2}E_p^2E_s^* ,$$

$$\frac{dE_s}{dz}+\left(\frac{\alpha}{2}-i\kappa|E_p|^2\right)E_s=\frac{i\kappa}{2}E_p^2E_t^* ,$$

where it is assumed that the linear absorption coefficient is the same for the test and signal beams. Indeed, that is not a restrictive hypothesis: As shown in Sec. III, in the cubic CuCl the absorption is the same for all the three beams and in the uniaxial CdS, for the configuration we have most extensively studied, all the polarizations are perpendicular to the optical axis $\hat{c}$ so that α is the same for all beams. For the other configuration, E_p is parallel to $\hat{c}$, E_t perpendicular to $\hat{c}$, then E_s is also perpendicular to $\hat{c}$ and $\alpha_t=\alpha_s=\alpha$. The solution for the intensities is written

$$I_p(z)=I_p(0)(\exp-\alpha z)/[1+\kappa_2 I_p(0)l_a], \tag{1a}$$

$$I_s(z)=I_t(0)(\exp-\alpha z)[\tfrac{1}{2}|\kappa|I_p(0)l_a]^2/[1+\kappa_2 I_p(0)l_a]^3, \tag{1b}$$

$$I_t(z)=\{I_t(0)(\exp-\alpha z)/[1+\kappa_2 I_p(0)l_a]^2\}+I_s(z)$$
$$=\tilde{I}_t(z)+I_s(z), \tag{1c}$$

where $l_a = [1 - \exp(-\alpha_p l)]/\alpha_p$ is the effective interaction length due to the pump linear absorption; it decreases from the sample thickness l to α_p^{-1} when α_p grows from zero to infinity. Let us discuss briefly this set of relations. For weak absorptions, one has $I_s(l) \propto |\chi^{(3)}|^2 I_p^2(0) I_t(0) l^2$ and $I_t(l) = I_t(0) + I_s(l)$. This is the usual parametric approximation of nonlinear optics. Now, in the case which we call hyperparametric, the pump is considered as if it propagated alone; it is seen from Eq. (1b) that the signal intensity results from the competition between the nonlinear gain, proportional to the squared modulus of $\chi^{(3)}$ and the TPA, governed by its imaginary part.

Equation (1c) also deserves some comment: the first part of the right-hand term represents the TPA induced by the pump and the second is the nonlinear gain; those terms are uncoupled. Now, most of the TPA experiments are performed in a two-beam configuration, where one measures the attenuation of a weak beam induced by a strong one; in other words, one measures $I_t(z)$. Up to now, the nonlinear gain has been overlooked and the data were analyzed by use of the only first part of Eq. (1). While that procedure is legitimate in the case of thick samples when the nonlinear gain is not phase matched, it is not in the case of thin samples. Actually, in some of our experiments it was found to be 10–50 % of the output test intensity. Therefore, a number of values, especially those concerning the TPA cross-section calibration, result from an improper interpretation of the data.

The hyperparametric approximation (HPA) provides us with an accurate quantitative description of FDFWM. By comparing the solution in the HPA and the numerical solution of the full system,[9] it is shown that, even at resonance on CuCl, the results of the HPA agree with those of the numerical calculation to better than a few percent (~3%) as long as $I_p(0) \gtrsim 5 I_t(0)$; actually, the two descriptions agree within a factor of 2–3 up to $I_p(0) \simeq I_t(0)$ (see Fig. 2 of Ref. 9). Therefore the analytical form Eq. (1) can safely be used to discuss the observed spectra. As will be seen in the forthcoming sections, the signal is very sensitive to the relative line shapes of $|\chi^{(3)}|$ and $\mathrm{Im}\chi^{(3)}$ and profit will be extracted from that sensitivity to get new results.

B. Third-order susceptibility

In order to proceed to a spectroscopic analysis of the signal intensity, it is necessary to have at our disposal an expression of the third-order susceptibility $\chi^{(3)}$ which can characterize the processes occurring in the crystal. In principle, all the processes which lead to a polarization third order in the fields and which have the proper frequency and wave vector should contribute to $\chi^{(3)}$. A number of authors[12] have derived formal expressions for $\chi^{(3)}$, but they are so complicated that from a practical point of view only in the case of simple systems such as alkali atoms[13] can they be used for numerical computations. In the case of solids it would be a formidable task to undertake such work and it is necessary to proceed to approximations towards tractable formulas. However, some caution should be taken in the choice of the approximations, since $\chi^{(3)}$ has to satisfy the necessary conditions for a triple causal Fourier transform[14] and thermodynamic inequalities.

For instance, concerning that latter point, a medium irradiated by a plane wave at frequency ω experiences such a TPA that the rate of absorbed energy is[15]:

$$\left\langle \frac{\partial}{\partial t} (\text{energy/volume}) \right\rangle = \tfrac{1}{2} \mathrm{Re}(-i\omega\chi^{(3)} |E|^4)$$

which implies that the imaginary part of that $\chi^{(3)}$ is a positive function.

In the current approximation a set of energy levels of the system is singled out because it is thought to have a preponderant contribution and the other ones are lumped together in a nonresonant background. Let us now examine in that respect the compounds we have investigated.

Cuprous chloride (CuCl) belongs to the $\bar{4}3m$ point group; its three crystallographic axes (1, 2, 3) are equivalent so that its nonlinear susceptibility has four independent components $\chi^{(3)}_{1111}$, $\chi^{(3)}_{1122}$, $\chi^{(3)}_{1212}$, and $\chi^{(3)}_{1221}$.

Cadmium sulfide (CdS) belongs to the $6mm$ point group; it is uniaxial crystal with two equivalent axes 1 and 2 perpendicular to the optical axis 3. It can be described by $\chi^{(1)}_{33}$ and $\chi^{(1)}_{11}$ $(= \chi^{(1)}_{22})$ for the linear susceptibility and by ten independent components for the third-order one[12]; they are $\chi^{(3)}_{3333}$, $\chi^{(3)}_{1111} = \chi_{2222} = \chi_{1122} + \chi_{1221}$, χ_{1122}, χ_{1212}, χ_{1133}, χ_{1313}, χ_{1331}, χ_{3131}, χ_{3311}, and χ_{3113}.

Schematic representations of the band structure and of the exciton and biexciton states of the two crystals are given in Figs. 2(a) and (b). The symmetry assignments of the states have been worked out by a number of authors and an exhaustive review can be found in the article by Bassani *et al.*[16] The one-photon allowed electric-dipole transitions are indicated by simple arrows and the corresponding two-photon ones by double arrows. It is apparent from an inspection of Fig. 2 that the lowest-energy biexciton states, which have in both compounds the same symmetry, Γ_1, as the crystal ground state will give rise to a two-photon resonance. In addition, the most substan-

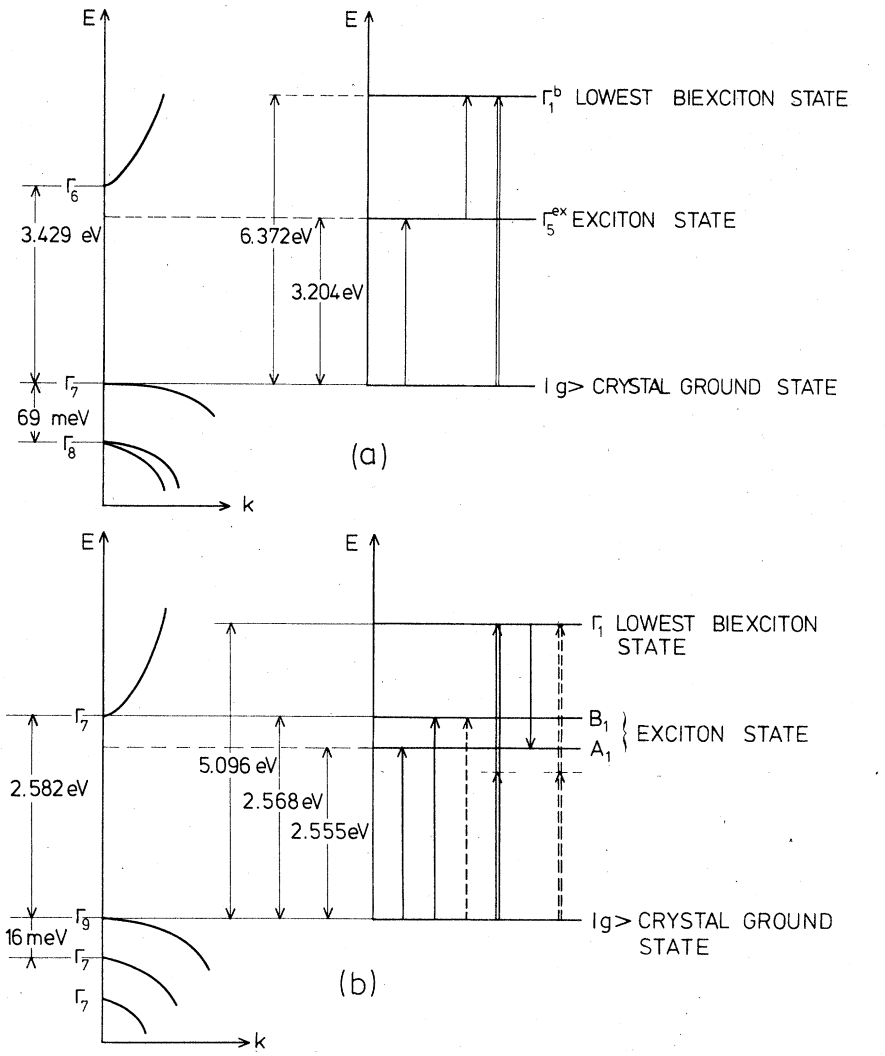

FIG. 2. (a) Schematic of the band structure of CuCl around Γ and of the relevant electronic transitions, with selection rules for the electric dipole. All the fields are parallel to the [001] axis which is in the plane of the surface sample. Simple arrows go with one-photon transition and double arrow goes with two-photon transitions. All numerical values are from the Strasbourg group [Refs. 5 and 6(a)]. (b) Schematic of the band structure of CdS around Γ and of the relevant electronic transitions, with selection rules. The full lines represent electric dipole-allowed transitions with the polarization of the electric field perpendicular to the c axis and the dotted ones those with polarization parallel to c axis. Simple arrows go with one-photon transitions and double arrows with two-photon transitions. But for the formation energy of the biexciton which is ours, all numerical values are from Planel [Ref. 7(e)].

tial contribution as intermediate states appears to come from the excitons whose energy is closest to half that of the biexcitons; those are the Z_3^T in CuCl and the A_1 or B_1, according to the polarizations, in CdS. It is therefore tempting to approximate the energy scheme of the crystals to that of a three- or a four-level system. In order to check the validity of this assumption, it is necessary to consider in detail the expression of $\chi^{(3)}$. Note that in all that follows, we shall neglect all the spatial dispersion effects. that point will be discussed in Sec. III.

The computation of the third-order susceptibility is by no means trivial; first, one has to solve the evolution equation of the density matrix

$$\rho = \sum_n \rho^{(n)}, \quad i\hbar \frac{\partial}{\partial t}\rho = [H_0 + H_1, \rho]$$

up to the right order, and then to isolate the terms having the right frequency. In the above equation, the interaction Hamiltonian, in terms of the electric dipole μ and electric field E is written H_1

$= -\vec{\mu}\cdot\vec{E}$. The general expansion of ρ has been thoroughly investigated; recently, Yee *et al.*[17] gave a diagrammatic technique, based on the Slichter formalism, which allows us to carry on the calculations in a systematic manner; Druet *et al.*[18] also discussed, through a pictorial diagrammatic technique approach, the line shapes associated with an electronic resonance in resonant CARS (coherent anti-Stokes Raman scattering). Starting from a different point of view, Hanamura[19] has independently developed a very similar formalism. Since the time evolution of both the wave function and its complex conjugate have to be considered in a separate way, there are in the development of $\rho^{(n)}$: $2^n(n)!$ terms, which, for $n=3$ (the necessary order for $\chi^{(3)}$) amount to 48. However, this number reduces to 24 when two of the fields are indiscernible, as is the case for the FDFWM.

The damping and the coherence losses are accounted for by statistical averaging of products of bra and ket propagators over the time intervals during which their evolution is correlated. The expectation value of the dipole moment is then calculated in the usual manner, and from the third-order dipole moment $\mu^{(3)} = \mathrm{Tr}(\mu\rho^{(3)})$ one extracts the expression of $\chi^{(3)}$. The calculation has been carried out for the degenerate four-wave mixing case; the 24 diagrams involved in $\rho^{(3)}$ as well as the full expression for $\mu^{(3)}(\omega)$ are given in the Appendix, with the following notations:

$$\hbar\Omega_{ij} = W_i - W_j - i\Gamma_{ij} = -\hbar\Omega_{ji}^{*},$$

where (i) W_i is the energy of the state $|i\rangle$, including possible collisional and light shifts; (ii) $\Gamma_{ij} = \frac{1}{2}(\Gamma_i + \Gamma_j) + \Gamma_{ij}^{c}$ where Γ_i is the inverse lifetime of level $|i\rangle$ and the damping constant Γ_{ij}^{c} describes elastic and inelastic collisions for levels $|i\rangle$ and $|j\rangle$; we define the diagonal component of $\hbar\Omega_{ij}$ as $\hbar\Omega_{ii} = -(i/2)(\Gamma_i + \Gamma_i^{c})$ in terms of the inverse lifetime and inelastic collision frequency Γ_i^{c}. For an isolated set of levels, one would have $\Gamma_i^{c} = \sum_{j\neq i}\Gamma_{ij}^{c}$.

Comparing the expression of $\mu^{(3)}$ and the energy schemes of Fig. 2, one immediately identifies a dominant term with three resonant-energy denominators, and arising from the contribution to $\rho^{(3)}$ of the diagram D_1 of Fig. 12,

$$\gamma_{3R} = \frac{\mathfrak{N}}{\hbar^3}\frac{\mu_{gl}\mu_{lm}\mu_{mj}\mu_{jg}}{(\Omega_{eg}-\omega)(\Omega_{mg}-2\omega)(\Omega_{jg}-\omega)},$$

where j and l refer to the dominant intermediate excitons and m to the excitonic molecule. Near the two-photon resonance, $2\hbar\omega \simeq W_{mg}$ and the denominator of γ_{3R} reduces approximatively to $i\Gamma_{mg}\Delta_B^2/4$ where Δ_B is the excitonic molecule binding energy, i.e., some meV. It would seem that another term has also a triply resonant denominator; this term, arising from diagram D_4 involves the energy difference between two excited states, i.e., $W_{mi} - i\Gamma_{mi} - \hbar\omega$, but this type of resonance would be very weak. This can be seen by collecting and summing all the terms in which it appears. Assume for instance that all the fields are parallel; then the sum of diagrams $D_4 + D_{11} + D_{18}$ leads after some algebra to the term

$$[\tfrac{1}{2}i(\Gamma_{mx} - \Gamma_{xg} - \Gamma_{mg}) + \tfrac{1}{2}i(\Gamma_{gx} + \Gamma_{xg} - \Gamma_{xx})(\Omega_{mg} - 2\omega)/\Omega_{xx}]/(\Omega_{mx} - \omega).$$

The necessary and sufficient condition for those terms to vanish is $\Gamma_{mx} = \Gamma_{xg} + \Gamma_{mg}$. Such is the case if Γ is due to radiative damping.[20]

Anyway, in the numerator appear differences of damping constants and since at resonance the denominator reduces to one damping constant, the contribution of those terms keeps small, for example, a vaguely structured background at most. The observation of resonances associated with energy differences between excited states, although the subject of intense investigation,[20] has not been performed up to now. In the case of solids they are most likely hidden in the nonresonant background arising from the other terms, and we will not consider them any more.

The terms which have the next dominant character are the doubly resonant ones (or excitons). They arise from diagrams of the D_1 type, with a second intermediate state different from $|m\rangle$ or from diagrams of the D_9 type, with any second intermediate state; they are written:

$$\gamma_{2R} = \frac{\mathfrak{N}}{\hbar^3}\left(\sum_{a\neq m}\frac{\mu_{gi}\mu_{ia}\mu_{aj}\mu_{jg}}{(\Omega_{ig}-\omega)(\Omega_{ag}-2\omega)(\Omega_{ig}-\omega)} + \sum_{a}\frac{\mu_{gi}\mu_{ia}\mu_{aj}\mu_{jg}}{(\Omega_{ig}-\omega)\Omega_{ag}(\Omega_{jg}-\omega)}\right).$$

In a three-level system (with perhaps a nearly degenerate intermediate state) only the terms in the second summation corresponding to $a=m$ appear. It is thus not possible to approximate the energy-level scheme of a crystal to that of a three or four-level system, if other contributions than that of the most dominant term have to be considered. There are also a number of single resonant terms such as those arising from dia-

grams D_3 and D_7 with any first and second intermediate states or from diagrams D_1, or D_9 with intermediate states different from $|m\rangle$ or $|x\rangle$, and finally a large number of nonresonant terms. (There are 11 nonresonant diagrams.) In order to see if we can use only the triply resonant term to describe the crystal third-order susceptibility, let us examine its dispersion. For simplicity, we consider only one intermediate exciton state and use the normalized and centered energy $\nu = (W_{mg} - 2\hbar\omega)/\Gamma_{mg}$; then the normalized exciton energy and linewidth are $\frac{1}{2}\Delta_B = (W_{xg} - W_{mg}/2)/\Gamma_{mg}$ and $\xi = \Gamma_{xg}/\Gamma_{mg}$. The imaginary part of the triply resonant term is proportional to

$$f(\nu) = \nu^2(1+2\xi) + 2\Delta_B(1+\xi)\nu + \Delta_B^2 - \xi^2 .$$

At the two-photon resonance, $f(0) = \Delta_B^2 - \xi^2$ is positive provided the excitonic molecule binding energy ($\Delta_B = \frac{1}{2}\Gamma_{x_2}\delta_B$) is larger than the exciton full linewidth. That is indeed the case if a molecule is effectively to be formed from two excitons. However, at the one-photon resonance on the exciton, $f(-\delta_B) = -\xi^2$ is always negative. The small region, $2\xi\delta_B$ large, around the exciton, over which $\mathrm{Im}(\chi^{(3)})$ is negative is indicative of the locality of our approximation. Now, one is interested in general in exploring some excitonic linewidth around the two-photon resonance. If the excitonic molecule binding energy is substantially larger that both the exciton linewidth and its own, then the crystal $\chi^{(3)}$ is safely approximated by γ_{3R}. As will be seen, such is the case for CuCl whereas CdS is much more troublesome in that respect.

Therefore, in compounds with rather large binding energies, a Lorentzian shape for $\chi^{(3)}$ should lead to a similar profile for the signal, with a nonlinear gain ($|\chi^{(3)}|^2$) wider than the signal depletion due to TPA [see Eq. (1b)]. At low intensity one should observe an essentially symmetric resonance; at higher intensity, TPA may dig a dip at its center. In both cases a small dissymmetry reflecting the smooth variation of the linear absorption may be evidenced.

In compounds with rather small binding energies, below the two-photon resonance energy $\hbar\omega \lesssim \frac{1}{2}W_{mg}$, the signal is mainly driven by the nonlinear gain (triply resonant term), but for $W_{mg}/2 \lesssim \hbar\omega \lesssim W_{xg}$ interferences between the doubly and triply resonant terms should be manifest, and the spectrum should be very sensitive to the relative signs and magnitudes of the respective numerators. Since, in addition, the linear absorption is large and very dispersive, no qualitative description of the resonance line shape can be given without numerical analysis.

II. FIRST-ORDER SCATTERING: THE AUTOIONIZING CHARACTER OF BIEXCITONS

A. Experimental procedure

A schematic of the experimental setup is given

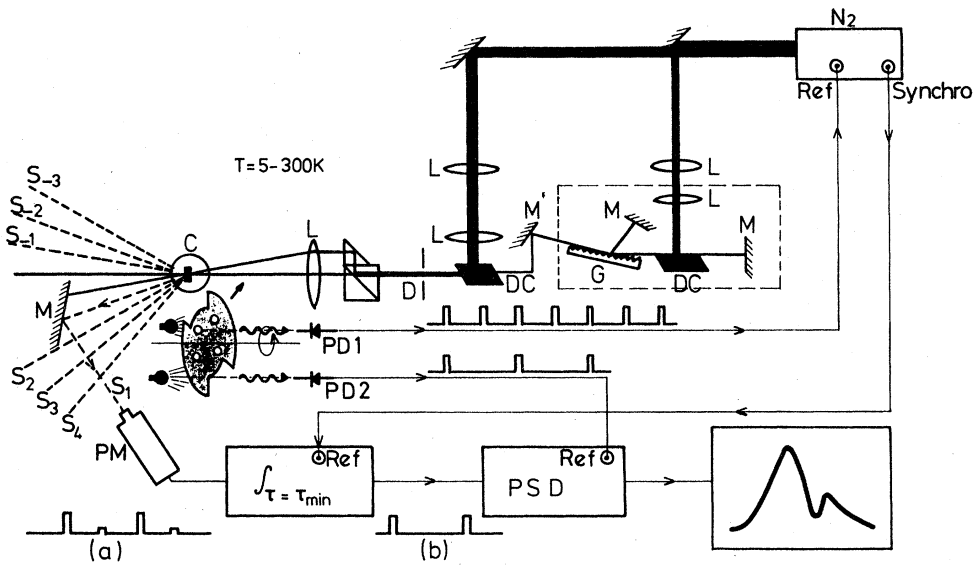

FIG. 3. Schematic of the experimental setup: L = lenses, DC = dye cells, G = grating, M = mirrors, C = cryostat, D = diaphragm, PM = photomultiplier, PSD = phase sensitive detector; the latter is preceded by a sampler integrator. The PD are the lamp-photodiode cells. The pump and test beams are represented by full lines, the successive diffraction orders by dotted lines. The double detection method is symbolized by the time dependence of the electric signals: one sees how, from (a) to (b), the structured noise arising mainly from the scattering of the pump beam on the various surfaces is subtracted from the total signal out of the photomultiplier.

in Fig. 3; as noted in the Introduction only one tunable laser is required. We have used an oscillator-amplificator dye laser system pumped by a nitrogen laser, model no. C950 of Avco (4-nsec duration and 200-kW peak power).

The tunable oscillator is built according to the design of Shoshan *et al.*[21] with a grazing incidence grating as dispersive element, enabling us to avoid the use of an intracavity beam expander. It is transversely pumped with slightly less then half of the N_2 laser output; the back mirror is mounted on a high-precision rotation stage actived by a stepper motor, 500 steps corresponding to one degree. Two dyes, both from Lambda Physik, were used, BbQ for operation around 3900 Å and Coumarin 152 around 4900 Å.

The oscillator is followed by a gain-5 amplifier (which is a cell identical to that of the oscillator) transversely pumped by the remaining part of the nitrogen laser output. For both dyes, the system gives a linearly polarized beam, with pulses 5-kW peak power 4-nsec duration and 0.3-Å linewidth.

A system of prisms splits the laser beam into two parts in the ratio 3 to 1, providing for the pump and test beams, respectively. The prisms are mounted on high-precision translation and rotation stages so that the beam separation and direction can be finely adjusted. Calibrated neutral density filters and $\frac{1}{2}\lambda$ quartz plate were used to vary the intensities and the polarizations. Finally, the beams are focused on the same point of the sample. According to the focal length, the spot waists on the sample can be chosen between 100 and 300 μm; the angle between the beams can be varied continuously from 0.5° to 5°.

The samples are either immersed in liquid helium or stuck on the copper cold finger of a variable temperature cryostat. In the latter case, the temperature of the copper finger is stable within 0.1 K from 10 to 120 K. For a precise positioning of the samples, the cryostats are mounted on an xyz translation stage. The samples are heated somewhat by the laser pulses. In order to estimate their actual temperature, we have calculated the maximum temperature rise at the center of the beam with Gaussian energy distribution, both in space and time, assuming that the specific heat was constant. It was found that, at the input face of the sample the increase of temperature with respect to that of the copper holder did not exceed 15 K. The signal beam is detected 80 cm from the sample by an S-20 photomultiplier preceded by a small (~2-mm diameter) hole; one is then sure that no luminescence of stimulated emission line is let through the detection system.

A key point in the experiment is to make the beams intersect and focus on the same point in the sample inside the cryostat. Now, an actual problem is that photons, mainly from the intense pump beam, are unavoidably scattered on the cryostat windows, the lenses, and the sample surface. Some of these scattered photons may have a component in the direction of the signal beam; with the same energy, momentum and polarizations, they are undistinguishable from it and cause a structured background. This background is subtracted by a double lock-in technique which relies on the fact the nonlinear signal is created only when the pump and test beams are simultaneously applied on the sample. The method is the following: A wheel with a set of two windows and a set of four holes, both regularly placed, is rotating at frequency 6 Hz; two lamp-photodiode sets are placed around the wheel providing with synchronization signals of frequency $f_p = 24$ Hz and $f_t = f_p/2 = 12$ Hz, the N_2 laser being triggered by the former. The wheel is placed in such a way that the pump beam goes through the holes at frequency f_p and the test beam through the windows, at frequency f_t.

The output of the photomultiplier feeds a sampling integrator (ATNE) triggered at frequency f_p and which has a time constant such that it lets through the low-frequency component of the signal (f_t) and quenches its high-frequency part (f_p). The output of that integrator is then a square wave, the higher value corresponding to the crossing of the pump and test beams interacting in the sample and the lower one to the spurious light scattered from the pump beam. The output

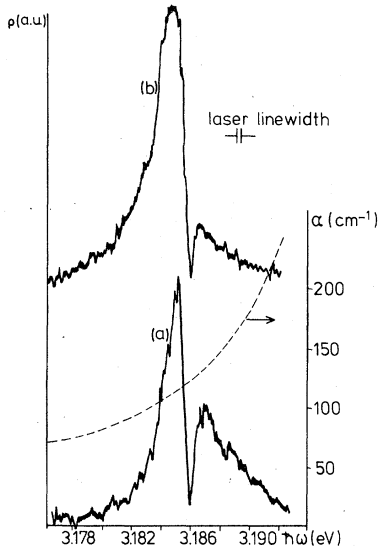

FIG. 4. First-order scattering spectrum in CuCl. (a) $l = 80$ μm, (b) $l = 200$ μm. Dashed line: absorption coefficient. In both spectra, the dip is located at half the formation energy of the biexciton.

of the sampling integrator feeds a lock-in amplifier (PAR 128) triggered at frequency f_t and which integrates the "ordinary" unstructured noise. Its output is eventually sent to a strip chart recorder.

This double-detection method was found to be highly satisfactory. Its efficiency is demonstrated in Fig. 7, the two upper lines correspond to recording of the signal in configurations discussed below, the lower one corresponds to the noise let through our detection chain when the two laser beams have been intentionally misaligned so that they do not overlap in the sample.

B. Experimental results

In cubic CuCl, only one polarization configuration has been investigated, namely $\vec{E}_p \| \vec{E}_t \| [001]$, then one measured $\chi^{(3)}_{xxxx}$; in uniaxial CdS two configurations have been investigated, the first one with $\vec{E}_p \| \vec{E}_t$, perpendicular to the $\hat{c}$ axis (then one measured $\chi^{(3)}_{xxxx}$) and the second one with E_p parallel and E_t perpendicular to that axis (then one measured $\chi^{(3)}_{xzzx}$). For all cases the polarization of the signal beam is identical to that of the test one. A very strong resonance is indeed observed in CuCl around $\hbar\omega = 3.186$ eV and in CdS for $\hbar\omega = 2.548$ eV.

Even at moderate intensities ($P_p \sim 1$ kW, $P_t \sim P_p/5$, $2W_0 \sim 200$ μm), the efficiency is such that it is very easy to observe with the naked eye either the fluorescence of a sheet of paper excited by the uv signal (CuCl) or the blue signal itself (CdS). The signal intensity exhibits a highly structured dependence on the laser frequency. Typical examples of the recorded spectra are shown in Figs. 4 to 7. Let us briefly comment on them:

CuCl: The spectra exhibit a central dip surrounded by two humps whose relative heights depend on the intensities, and on the sample thickness. The ratio of the height of the high-energy maximum to that of the low-energy one varies from 0.5 to 0.2, according to our experimental conditions. The full line-width increases with sample thickness and initial powers; the two maxima undergo slight red and blue shifts, respectively, for the low- and high-energy maxima.

CdS: The same features are observed as concerns linewidth and position of the maximum, but the dip can only be evidenced at higher intensities and for thick samples. That latter point is not a surprise since according to the hyperparametric approximation the only relevant external parameter is $I_p(0)l_a$, which for low absorptions identifies with $I_p(0)l$. Both power densities and sample thickness are lumped into the product of one unique quantity. In that case, the low-energy maximum is substantially broadened and its height is more than one order of magnitude greater than that of the high-energy one, which happens in some cases to be no more than a bump.

At moderate intensities, the resonance appears as a dissymmetric peak with its maximum substantially shifted towards the low-energy side of the previous dip (Fig. 5). Figure 7 shows two runs recorded in the same conditions, but for the pump beam polarization which was rotated 90° by a $\lambda/2$ plate. The spectra have been translated for convenience but they are very similar indeed. Finally, the temperature dependence of the signal was investigated, with no spectacular results with regard to our purpose: with increasing temperature, one observes a smooth decrease of the signal in-

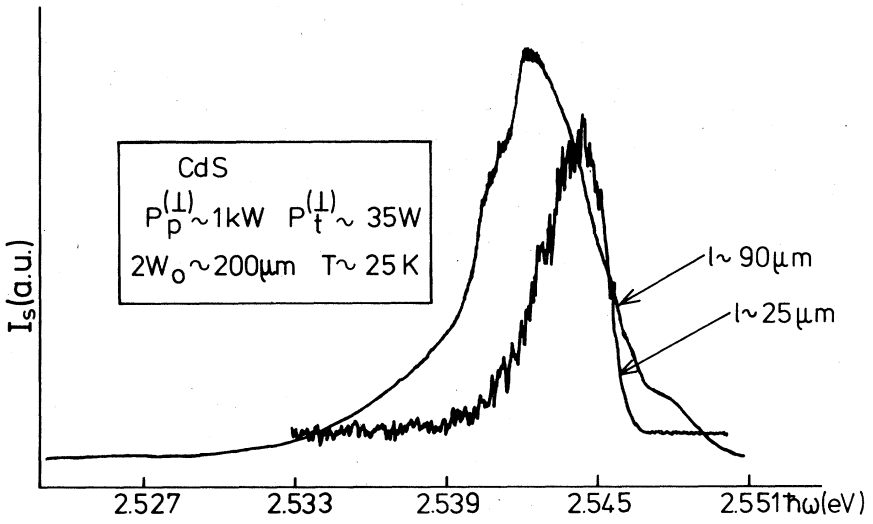

FIG. 5. Sample thickness dependence of the first-order scattering in CdS.

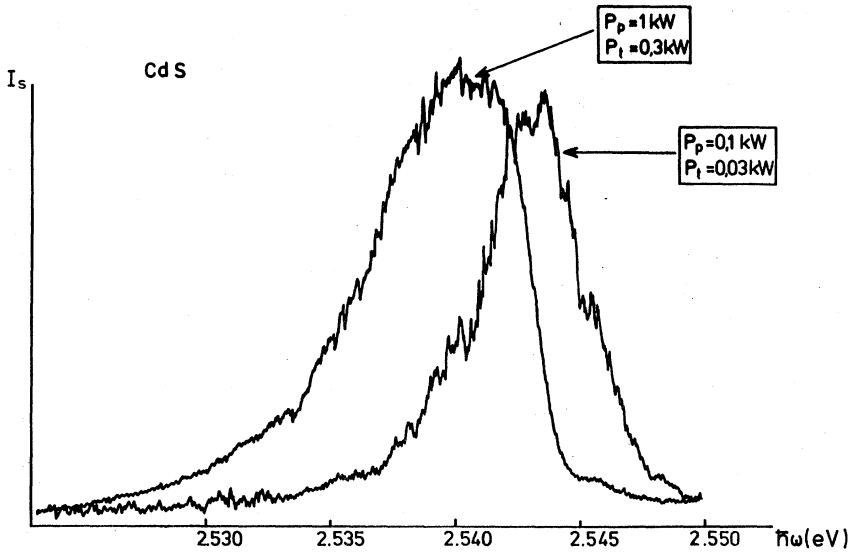

FIG. 6. Power dependence of the first-order scattering in CdS for a 80-μm-thick sample. All beams perpendicular to c axis.

tensity, and a corresponding increase of the linewidth. The intensity of the resonance peak varies as indicated as shown in Fig. 8.

Were it but one dissymetric peak, the description of the biexciton as a discrete level would be a very sound basis for the description of $\chi^{(3)}$ provided that, as indicated in the preceding section, one accounts properly for the excitonic quasiresonances. The existence of two peaks with intensity-dependent ratios and distance contradicts that description.

A number of explanations such as polariton ef-

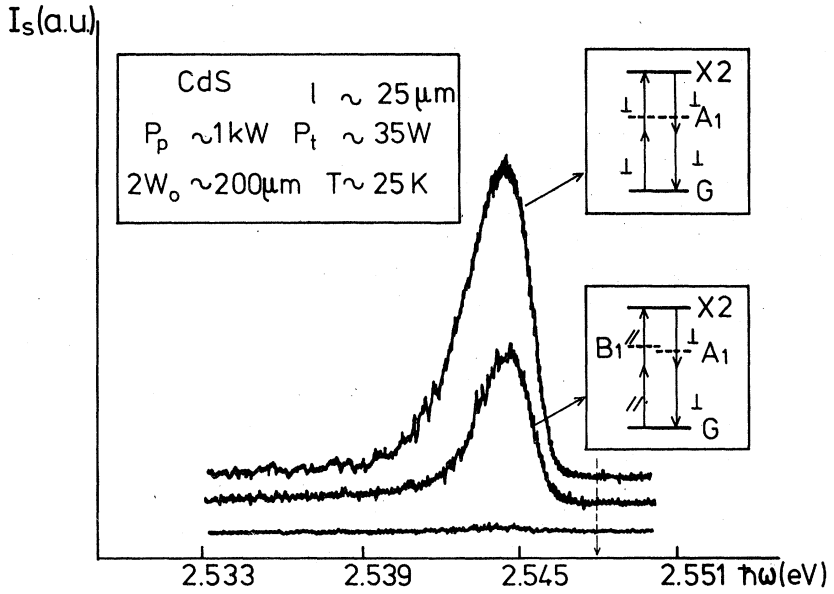

FIG. 7. Polarization dependence of the first-order scattering spectrum. Upper curve: all perpendicular configurations. Middle curve: Upward transitions are with beams polarized parallel to the c axis (pump); downward transitions are with beams polarized perpendicular to the c axis (test and signal). The curves are at the same scale and have been translated for convenience. The lower curve is obtained after a slight misalignment of the exciting beams; it corresponds to the remainder of parasite phenomena (diffusion on surfaces, luminescence, etc.) and has been also translated for convenience: it actually sticks to the base line. The arrow points to the position of the resonance, thus evidencing the importance of the propagation effects.

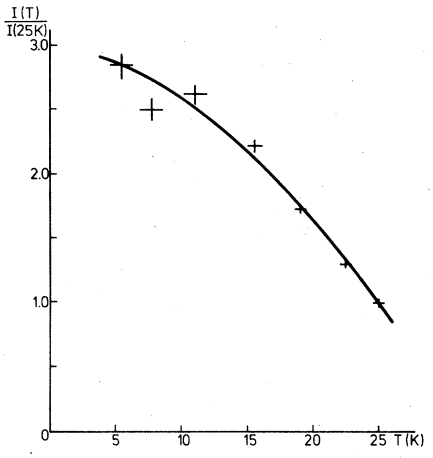

FIG. 8. Intensity of the maximum of the first-order scattering as a function of the temperature of the cold finger of the cryostat.

fect are easily ruled out by simple examination of the magnitudes of the shifts and the splittings. The only possibility left is that TPA is not the same on each side of the resonance. Such a behavior is, for a two-photon process, the analog of a Fano's interference effect on an autoionizing resonance for one-photon processes. This point is examined in detail now.

C. Autoionizing character of biexcitons

Excitonic molecules are usualy considered as bound states with respect to two free excitons.[4] But they are metastable states which decay spontaneously and the most probable recombination path is through the emission of two free polaritons.[21] This free pair forms a continuum whose energy overlaps that of the excitonic molecule, and which is coupled to it. Such a coupling results in a quantum interference which modifies deeply the nature of the system. In addition, since $W_{mg} \simeq 2E_g$ there is a very large density of excited crystal states whose energy overlap that of the biexciton and which may eventually be coupled to it. The problem of the coupling of a continuum and a discrete state has received a lot of attention in atomic and solid-state physics, for a one-photon process.[23] Autoionizing effects in nonlinear optics have been investigated in metal vapors[24] (for one-photon transitions) but, to the best of our knowledge, never in the solid state. In the remainder of this paragraph, we shall quote the most salient results of that coupling, adapt Fano's formalism to the description of excitonic molecule, and develop a model for the third-order susceptibility describing the degenerate four-wave mixing when the system under study involves a two-photon autoionizing resonance.[8]

Let $|m\rangle$ be the ket corresponding to the bare excitonic molecule, with energy W_m and $V(\epsilon)$ the coupling operator between this discrete state and the continuum $|c(\epsilon)\rangle$. The discrete state gets dressed, its energy becomes, after coupling, W_{x2}, and the ket corrresponding to that new state is written

$$|x_2\rangle = |m\rangle + \mathcal{P}\int \frac{V(\epsilon')}{\epsilon - \epsilon'} |c(\epsilon')\rangle d\epsilon' .$$

We call biexciton the dressed state. The true quantum state with energy ϵ in the crystal is a linear combination of the dressed discrete state and the continuum; following Fano's notations, it is written

$$|b(\epsilon)\rangle = \frac{\sin\Delta}{\pi V^*(\epsilon)} |x_2\rangle - \cos\Delta\, |c(\epsilon)\rangle .$$

We call bipolariton this true quantum state. The relevant feature of the function $\Delta(\epsilon)$ is that it varies from 0 to π when the discrete state energy is crossed. It is important at this point to remark that the transition probability from the exciton x_j to the bipolariton vanishes in the vicinity of the resonance, for an energy W_0 and an angle Δ_0 such that[23]

$$\cot g\Delta_0 = q(W_0) = \frac{\langle x_2|\mu|x_j\rangle}{\pi V^*(W_0)\langle c(W_0)|\mu|x_j\rangle} .$$

Such a relation neglects the possible coupling between states of the continuum; nevertheless, it can be shown[23] that the transition amplitude although not vanishing becomes very small around that value. The above relation defines the Fano parameter

$$q(\epsilon) = \langle x_2|\mu|x_j\rangle / \pi V_\epsilon^* \langle c(\epsilon)|\mu|x_j\rangle$$

which is infinite for a zero coupling. The strength of the coupling between the biexciton and the shell of states in the nearby continuum is actually given by the broadening:

$$\Gamma(\epsilon) = 2\pi |V(\epsilon)|^2 .$$

The new point concerning the computation of $\chi^{(3)}(\omega;\omega,\omega,-\omega)$ when a bipolariton is involved as a resonant intermediate state is that the summation on that previously discrete state has to be replaced by an integral over ϵ; one is led to compute such quantities as

$$\gamma_{jk}=\lim_{\eta\to 0^+}\int \frac{\langle g|\mu|x_j\rangle\langle x_j|\mu|b(\epsilon)\rangle\langle b(\epsilon)|\mu|x_k\rangle\langle x_k|\mu|g\rangle}{(W_{xj}-i\Gamma_{xj}-\hbar\omega)(\epsilon-i\eta-2\hbar\omega)(W_{xk}-i\Gamma_{xk}-\hbar\omega)}\,d\omega\,,$$

where the x_i refer to exciton states.

Following the assumptions of Fano we consider all numerators in that integral as constant; this implies that, around the two-photon resonance, the dipole matrix elements are constant, as well as $q_j(\epsilon)$, $V(\epsilon)$, and all densities of states.

While those hypotheses are not unrealistic for the matrix elements, they mean that all the dispersion of $V(\epsilon)$ is lumped into one unique parameter for each type of transition. This reminds us of the Debye temperature which lumps in one unique parameter all the dispersion of the phonons. The only integral to be performed is then:

$$\sigma_{jk}=\lim_{\eta'\to 0}\int \frac{(q_j+\epsilon')(q_k+\epsilon')}{(1+\epsilon'^2)(\epsilon'+\nu-i\eta')}\,d\epsilon'$$

$$=\pi\left(\frac{(q_j-i)(q_k-i)}{\nu-i}+i\right),$$

where a normalized energy scale has been introduced such that $\epsilon'=(\epsilon-W_{x_2})/\pi|V_E|^2$ and $\nu=(W_{x_2}-2\hbar\omega)/\pi|V_E|^2)$. One has

$$\gamma_{jk}=\sigma_{jk}\frac{\langle g|\mu|x_j\rangle\langle x_j|\mu|c(\epsilon)\rangle\langle c(\epsilon)|\mu|x_k\rangle\langle x_k|\mu|g\rangle}{(W_{xj}-i\Gamma_{xj}-\hbar\omega)(W_{xk}-i\Gamma_{xk}-\hbar\omega)}$$

for the scheme of levels indicated in Fig. 1.

It is advisable at this stage to compare the above expression to the one which is obtained when any autoionizing character is ignored. Call the latter $\gamma_{jk}=\gamma_{jk}^{\rm dis}$ and for simplicity let $\Gamma_{x_2}=2\pi|V(W_{x_2})|^2$. The meaning of that simplification is that the preponderant broadening mechanism is that due to the specific continuum whose kets are labeled by $|c(\epsilon)\rangle$. (Of course, there exist other continua which have negligible contributions in the broadening.) Then,

$$\gamma_{jk}=\gamma_{jk}^{\rm dis}\left(1-\frac{i}{q_j}-\frac{i}{q_k}+i\,\frac{W_{x_2}-2\hbar\omega}{q_jq_k\Gamma_{x_2}}\right), \tag{2}$$

$$\gamma_{jk}^{\rm dis}=\frac{\langle q|\mu|x_j\rangle\langle x_j|\mu|x_2\rangle\langle x_2|\mu|x_k\rangle\langle x_k|\mu|g\rangle}{(W_{xj}-i\Gamma_{xj}-\hbar\omega)(W_{x_2}-i\Gamma_{x_2}-2\hbar\omega)(W_{xk}-i\Gamma_{xk}-\hbar\omega)}\,. \tag{3}$$

It is seen from (2) and (3) that γ_{jk} reduces to $\gamma_{jk}^{\rm dis}$ for a weak coupling, (i.e., when $q\to\infty$). Note that up to now, the consequences of the autoionizing character of the bipolariton have been ignored and the data have been analyzed as if one dealt with a discrete level. While that provided an acceptable value for Γ_{x_2}, it overlooked dramatic effects due to the noninfinite value of q, as we emphasize now.

In order to discuss in more detail the consequences of our model for what concerns line shapes and spectra, we shall envision the two cases $j=k$ and $j\neq k$. In the first case, only one intermediate exciton plays a part, Z_3^T in CuCl or A_1 in CdS in the $(\perp,\perp)$ configuration. The triply resonant part of the third-order susceptibility is written

$$\chi_{\rm AI}^{\rm res}=\chi_{\rm dis}^{\rm res}\left[1-2i/q+i(W_{x_2}-2\hbar\omega)/q^2\Gamma_{x_2}\right],$$

where $q=q_j=q_k$.

Provided that q is much larger than unity, it is seen at once that $|\chi_{\rm AI}|^2$ and $|\chi_{\rm dis}|^2$ are equal up to a $1/q^2$ term. That shows that both models correspond to the same nonlinear gain with a Lorentzian line shape. But our point was a dissymmetric TPA. The TPA cross section in the autoionizing model is proportional to

$$\mathrm{Im}(\chi_{\rm AI}^{\rm res})\propto(\nu-q)^2/(1+\nu^2)$$

which is the well-known Fano-Beutler profile. It vanishes for $\nu=q$ $[\hbar\omega=\frac{1}{2}(W_{x_2}-q\Gamma x_2)]$ and is maximum for $\nu=q^{-1}$ $[\hbar\omega=\frac{1}{2}(W_{x_2}-\Gamma_{x_2}/q)]$.

As seen in Fig. 9 that profile is very dissymmetric indeed. Then the effect of q is to redistribute the modulus of $\chi^{(3)}$ between its real and imaginary parts. More precisely, $\mathrm{Re}\chi_{\rm AI}^{\rm res}\propto[(q^2-1)\nu+2q]/(\nu^2+1)$ which extrema are for $\nu_+=(q+1)/(q-1)$ and $\nu_-=\nu_+^{-1}$. Those two frequencies correspond to the half maximum points of $\mathrm{Im}(\chi^{(3)})$. The full half-width half maximum of $\mathrm{Im}(\chi_{\rm AI}^{\rm res})$ and thus of the TPA is $\hbar(\omega_+-\omega_-)=\Gamma_{x_2}(q^2+1)/(q^2-1)$ which is a decreasing function of q, equal to Γ_{x_2} only for large values of q.

The above remarks enable us to describe most easily the general features of the observed spectra. For $q\simeq$ some units, the nonlinear gain is

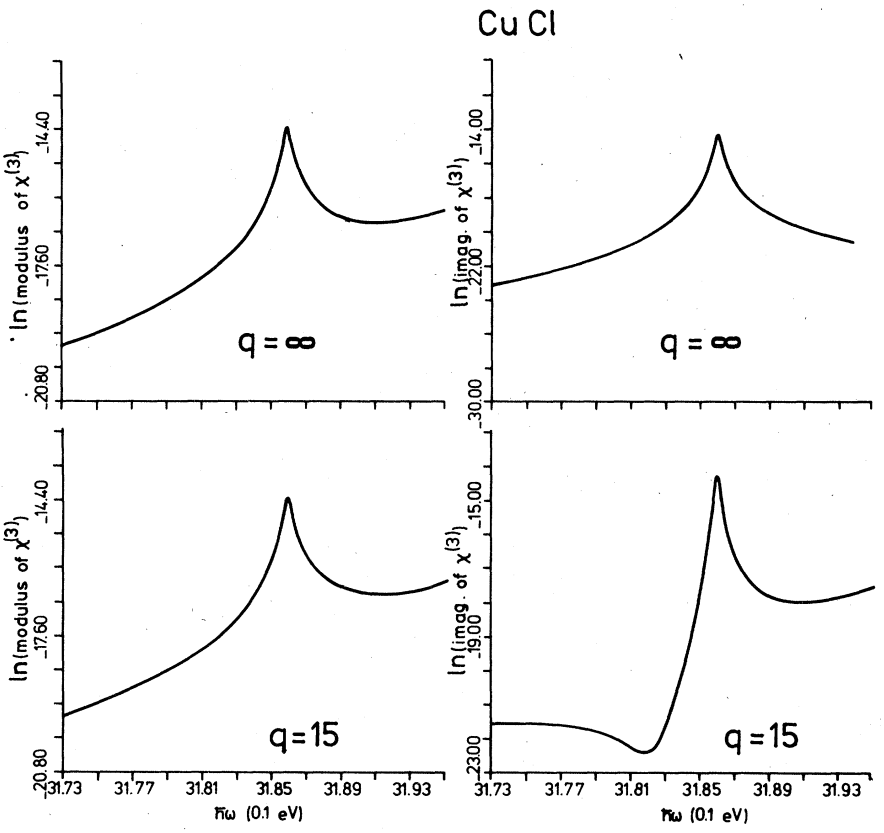

FIG. 9. Modulus and imaginary part of the third-order susceptibility in CuCl, in logarithmic units. The two upper curves correspond to the case of null coupling and the lower ones to the actual case. Note the identity of moduli in either case, and the differences between the imaginary parts (shape and numerical values). At resonance, the two-photon absorption coefficient, for $q=15$, is found to be $\beta = 55$ cm MW^{-1}. The shape of $\mathrm{Im}(\chi^{(3)})$ for $q \neq \infty$ is of the Fano-Beutler type.

almost symmetric and can be experienced even quite far from resonance because, as is the case for the Lorentzian profile, the width of $|\chi^{(3)}|$ is larger than that of $\mathrm{Im}|\chi^{(3)}|$.

Near resonance, for high intensities and (or) large sample thicknesses, TPA strongly depletes the pump and test beams, so that the generated signal drops to very low levels, giving rise to a central dip, whose width is approximately that of $\mathrm{Im}(\chi^{(3)})$. On each side of the dip, the symmetric gain is competing with the dissymmetric TPA, resulting in the two humps whose relative heights are governed by the term $\kappa_2 I_p^0 l_a$; they depend on the intensity and the length and reflect the dissymmetry of $\mathrm{Im}(\chi^{(3)})$.

For moderate intensities and thin samples, TPA is not efficient enough to overcome the nonlinear gain, the central dip disappears, and the resonance spectrum is a dissymmetric peak with a steep edge on the large-TPA side.

In the second case, which corresponds to CdS for a pump polarization parallel to the optic axis and test and signal ones perpendicular to it, the dipole matrix element for the A_1 exciton is not active for the pump. The next closest intermediate quasiresonance allowed for $E_p \| \hat{c}$ is the B_1 exciton. The leading term of $\chi^{(3)}$ is then

$$\chi^{\mathrm{res}}_{\mathrm{A\,I},xzzx} \propto \frac{\langle g|\mu_x|B_1\rangle\langle B_1|\mu_z|x_2\rangle\langle x_2|\mu_x|A_1\rangle\langle A_1|\mu_x|g\rangle}{(W_{B_1}-i\Gamma_{B_1}-\hbar\omega)(W_{x_2}-i\Gamma_{x_2}-2\hbar\omega)(W_{A_1}-i\Gamma_{A_1}-\hbar\omega)}\left(1-\frac{i}{q_{A_1}}-\frac{i}{q_{B_1}}+i\frac{W_{x_2}-2\hbar\omega}{q_{A_1}q_{B_1}\Gamma_{x_2}}\right).$$

It so happens that in both configurations for the pump, the signal intensity is roughly the same: in the first case $\chi^{(3)}$ is triply resonant but linear absorption is large (on A_1 exciton); in the second

one $\chi^{(3)}$ is only doubly resonant but residual absorption is much lower. We now derive benefit from all those remarks for the analysis of the experimental results.

III. ANALYSIS OF THE EXPERIMENTAL DATA

A. Biexciton parameters in cuprous chloride

Part of the corresponding discussion has been reported in a previous article[8] and is not reproduced here. Two of the biexciton parameters, its energy W_{x_2} and its linewidth Γ_{x_2}, are easily deduced from a direct inspection of the spectra. They are respectively, twice the energy of the central dip and its width. The relevant levels are therefore well separated and narrow, so that the three-level autoionizing approximation discussed in the previous paragraph is expected to be valid. Then the only two parameters to be fitted are the ratio between the oscillator strength of the exciton-biexciton transition to that of the ground-state-exciton one, $R = f_{xx_2}/f_{gx}$, and the Fano parameter q. The first one mostly drives the intensity of the signal and the second one its line shape. We have used a visual fitting procedure using the full set of six coupled equations; since the refractive index varies smoothly in the region of our spectra we have considered it (and the reflectivity as well) as constant. The absorption coefficient was measured and fitted to an analytical expression which was included in our computer program. However, it was found that taking it as a constant equal to its mean value did not alter significantly the line shapes. The experimental variable parameters are the sample thickness and the intensity $I_p(0)$ and $I_t(0)$. Note that even with one sample thickness, fitting all the spectra with different initial intensities is a rather severe check of our model. The best fit was always obtained with the same set of parameters, $R = 1000$, $q = 15$, indicative that we have access to intrinsic values of the semiconductor. This rules out, by the way, the possibility that the line shape might result from an interference of the resonant part of $\chi^{(3)}$ with some constant background. The results are shown in Fig. 10; the dotted curve of the upper diagrams shows the best fit we could obtain by putting $q = \infty$, i.e., assigning to $\chi^{(3)}$ a Lorentzian line shape. This point is very demonstrative of the very high sensitivity of our method. The dissymmetry of a Fano-Beutler profile can be defined as $\delta = 1 - \Delta^H/\Delta^L$, where Δ^H is the difference between the TPA maximum and its high-energy value, and Δ^L the corresponding quantity for the low-energy value. One can show that $\delta = (1+q^2)^{-1}$, i.e., $\simeq 4 \times 10^{-3}$ in the case of CuCl. The dissymmetry of $\mathrm{Im}\chi^{(3)}$ on a linear scale is

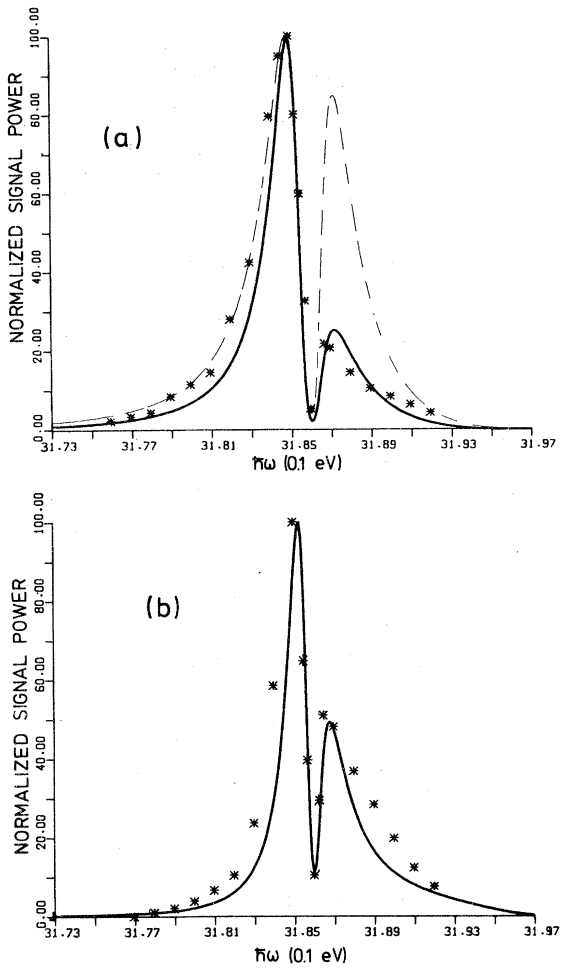

FIG. 10. Comparison of the experimental results for CuCl (asterisks) with those of theoretical models. (a) Dotted line: best fit for a 200-μm-thick sample, disregarding the autoionizing character of the biexciton. Full line: same computation, but considering the coupling with one continuum. (b) The full line corresponds to a 80-μm-thick sample, with the same parameters as above ($q = 15$).

difficult to evidence, and it needs to be dramatized on a logarithmic scale. This is shown in Fig. 9, where we compare the logarithms of $|\chi^{(3)}|$ and $\mathrm{Im}\chi^{(3)}$ of CuCl, for the Lorentzian and the autoionizing models. Such a small dissymmetric line shape is very difficult to observe, by noncoherent processes, especially amidst a large linear absorption background. It has to be noted, however, that they were observed by Ueta *et al.*[25] and interpreted by Hanamura[4] as arising from complex collisional broadening of the excitonic molecules actually created in a TPA experiment. Svorec and Chase[7(d)] also reported dissymmetry in the TPA profile but their discussion is only qualita-

tive.

Our fitted linewidth is $\Gamma_{x_2}=0.5$ meV. Let us remark that one can expect that q and Γ_{x_2} should vary in opposite manners, since the stronger the coupling is, the more efficient the decay. It corresponds to a TPA coefficient at resonance $\beta \simeq 55$ cm MW^{-1}. The value of R is in satisfactory agreement with the experiments of Phach *et al.*[26] and the theoretical estimates of Arya and Hassan[27] and of Ekardt and Sheboul[28] as previously discussed.[8] This very large value goes in the expected sense, according to the general trends of the exciton-complexes theory.[29]

Finally we have compared the fit obtained by numerical integration to that obtained by use of the hyperparametric approximation analytical solution, i.e., Eqs. (1). No difference in the quality of the fits could be noticed, with of course a tremendous gain in the simplicity and computer time for the latter procedure. As a consequence we only used the hyperparametric approximation solution in the forthcoming analysis.

B. Biexciton parameters in cadmium sulfide

Since the publication of preliminary results,[30] some improvements have been brought to the experimental procedure. First the characteristics of the laser have been improved, i.e., smaller linewidth and better control and reproducibility of the power densities. Such care had to be taken for a quantitative analysis because of the extreme nonlinearities of the signal. Then we systematically used a set of polarizers and an analyzer to control the polarization of the generated signal.

Three samples were investigated, with respective thicknesses 25, 80, and 90 μm. For each of them the absorption coefficient α has been measured at low temperature for both polarization $E \| \hat{c}$ and $E \perp \hat{c}$. The analysis has been detailed on the two samples which manifested the lowest absorption, i.e., $\alpha_\perp \simeq 200$ cm^{-1} and $\alpha_\parallel \simeq 50$ cm^{-1}, near $\hbar\omega = 2.545$ eV where the signal intensity is maximum. This region corresponds to that of the I_2 bound-exciton complex in CdS; we have checked that no saturation of this line could be observed up to 2.5 MW cm^{-2}. This is in qualitative agreement with the observation of Ref. 7(d) which gives a saturation intensity about twice our maximum value.

The case of CdS is much more complicated than that of CuCl owing to a smaller biexciton binding energy and the two possible intermediate exciton states. Our goal for the fitting procedure has been to describe correctly the main features of the spectra while keeping the maximum of simplicity in the analysis. In particular, we have tried to limit severely the number of unknown parameters feeding the computer program.

C. Configuration with all the polarization perpendicular to the optical axis

The analysis made use of the hyperparametric solution, taking into account the measured absorption coefficient and the dispersion of the refractive indices and of the reflectivity, according to the data of Jackel and Mahr.[31] The closest exciton intermediate state is the A_1 exciton, which is about 13 meV below the B_1 exciton. However, this latter state is active for $E \perp \hat{c}$ and rigorously one should write $\chi^{(3)} = \chi^{(3)}_{A_1} + \chi^{(3)}_{B_1} + \chi^{(3)}_{A_1-B_1}$ where:

$$\chi^{(3)}_{A_1} = \frac{|\langle g|\mu|A_1\rangle\langle A_1|\mu|x_2\rangle|^2}{D_{x_2}D^2_{A_1}}\left(1-\frac{2i}{q_{A_1}}+\frac{W_{x_2}-2\hbar\omega}{q^2_{A_1}\Gamma_{x_2}}\right),$$

$$\chi^{(3)}_{B_1} = \frac{|\langle g|\mu|B_1\rangle\langle B_1|\mu|x_2\rangle|^2}{D_{x_2}D^2_{B_1}}\left(1-\frac{2i}{q_{B_1}}+\frac{W_{x_2}-2\hbar\omega}{q^2_{B_1}\Gamma_{x_2}}\right),$$

$$\chi^{(3)}_{A_1-B_1} = 2\,\frac{\langle g|\mu|A_1\rangle\langle A_1|\mu|x_2\rangle\langle x_2|\mu|B_1\rangle\langle B_1|\mu|g\rangle}{D_{A_1}D_{x_2}D_{B_1}}\left(1-\frac{i}{q_{A_1}}-\frac{i}{q_{B_1}}+\frac{W_{x_2}-2\hbar\omega}{q_{A_1}q_{B_1}\Gamma_{x_2}}\right).$$

In these equations the energy denominators are noted D_j. The third-order susceptibility depends on a rather large number of unknown parameters and we have tried to reduce this number by putting $\chi^{(3)} = \chi^{(3)}_{A_1}$. Then the unknown parameters are W_{x_2}, Γ_{x_2}, q_A, and $R = f_{A_1x_2}/f_{gA_1}$. Among these, a rough estimate of Γ_{x_2} is given from the signal linewidth at lowest intensities and for the thin sample, while $\frac{1}{2}W_{x_2}$ is approximately given by the position of the energy dip of the spectra, when it can be seen, i.e., for the thicker samples and at high intensities. The justification of the approximation for the form of $\chi^{(3)}$ is made legitimate later on. The visual fitting procedure was found to be much more complicated than for CuCl. In that case only two parameters were involved, one was optimized in a run, then the other one; then we proceeded to a slightly reoptimization of the first,

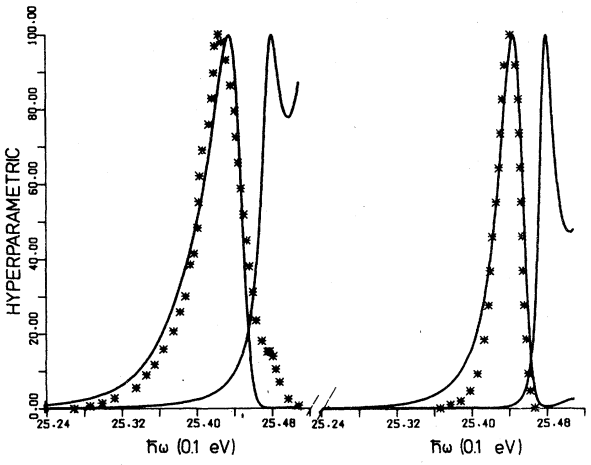

FIG. 11. Comparison of the experimental data (asterisks) and theoretical fits (straight lines) in the hyperparametric approximation for uniaxial CdS. Left part: 80-μm-thick sample. Right part: 25-μm-thick sample. The other curves represent, respectively, the modulus and the imaginary part of $\chi^{(3)}$. Note the shifts between the maxima of the spectra and that of $\chi^{(3)}$. Numerical values are given in the text. We have adopted the same numerical values for the damping constants of the samples even from different origins.

and after a small number of runs the final values were obtained. In the case of CdS, all the parameters affected both the position and the line shapes, which were also found to be quite sensitive to the exciton linewidth Γ_x. In fact the right set of parameters has to be found practically at once.

Typical results are shown in Fig. 11; the same fit quality was kept for the two samples and all the intensities with the same set of parameters. Although one can observe that the fits are somewhat better on the low-energy side of the spectra we think that, considering the approximations made for the analysis, those results are most satisfactory. Figure 11 also shows the modulus and the imaginary part of $\chi^{(3)}$; indeed they peak a few meV above the signal maximum, evidencing the necessity of an accurate account of the propagation effects for data processing. The parameters corresponding to the best fit are:

The biexciton energy: $W_{x_2}=5.096$ eV. [In the calibration of our monochromator we made use of spectral lamps, and used for the energy-wavelength conversion the relation $\lambda(\mu\text{m})\times\hbar\omega$ (eV) $=1.239\,51$]. This value compares satisfactorily to that reported by Planel *et al.*[7(c)] (5.099 eV at 1.6 K), Itoh *et al.*[7(g)] (5.1001 eV at 1.6 K), and Schrey *et al.*[7(c)] (5.098 eV at 5 K), especially if one realizes that the temperature of our samples was at least around 15 K. As suggested to us by Planel, it is possible to determine accurately the surface temperature of our sample by recording the crystal reflectivity synchronously with the dye laser pulses. However, for an accurate account of the temperature effect it would be necessary to know the temperature profile within the sample along the light path. Such a refinement is far beyond the accuracy we claim.

The biexciton linewidth: $\Gamma_{x_2}=1.8$ meV. This value is about four times larger than that found in the case of CuCl. That is not unexpected and is most likely related to the neglect of the spatial dispersion in the intermediate exciton state. It is well known that CdS is a standard semiconductor for the demonstration of that effect. From Tait's criterion[32] and our linewidth values, one can see that it is legitimate to neglect it in CuCl and that it is not in CdS. Our value is therefore most likely overestimated. Note that Levine *et al.*,[33] in their fit of tunable second-harmonic generation in CdS, found that the damping constants were one order of magnitude smaller in the polariton formalism than in the classical-exciton-theory formalism.

Nevertheless, it is noteworthy that the wave functions needed to describe the polariton in the spectral region we have investigated are mostly of the exciton type[34] and that $\chi^{(3)}$, as we have described it, is not affected by the spatial dispersion effect. The problem of the auxiliary conditions, which is very complicated in one-photon optics[35] is hardly tractable in nonlinear optics.[36]

The exciton-biexciton oscillator strength: We have found that $R=f_{A1x_2}/f_{gA_1}=2.3\times10^4$. To the best of our knowledge this is the first determination of that quantity. It is about 20 times as large as that of CuCl, in qualitative agreement with the general trends of exciton-complexes theory.[29] Indeed R is primarily determined by the spatial extension of the biexciton envelope function, and the smaller the binding energy ($\Delta_B=14$ meV for CdS and $\Delta_B=36$ meV for CuCl) the greater is the extension. However, the value of R may be overestimated as a result of the neglect of the B_1 exciton contribution.

The Fano parameter: $q_A=6$. This is quite a small value, indicative of a strong coupling between the biexciton and the continuum. That point raises the question of neglecting its dispersion, $q(\epsilon)$, in the Fano formalism, but this is related to the identification of the continuum and the coupling mechanism. The first candidates for the continuum are obviously the free pairs of polaritons and the conduction-band states. As for the coupling, one can consider the electron-phonon and the electromagnetic one. The study of the

question deserves supplementary experiments, including a careful description of the temperature dependence of the spectra. It is momentarily left for future studies.

It is worth noting that we have not included in our $\chi^{(3)}$ any doubly resonant terms or any dispersionless background. It was found during the numerous fitting tests that a term doubly resonant on the A_1 exciton, with an imaginary numerator nearly equal to the modulus of $\chi^{(3)}$ at resonance, noticeably improves the fit, whereas any real numerator is useless. Let us note that Bloembergen *et al.*[19] interpreted very simply some experimental data by adding to a resonant term a background whose value was 1.5 times that of the resonant part. However, because of the huge number of potential intermediate states for CdS, we feel that including another term in $\chi^{(3)}$ would be a sort of pure computer game obscuring the physics even if it improves the fits. In addition, one would never be sure that the parameters determined in such a way would be the unique set, whereas we can take for granted that those we have determined represent reasonable values of the true crystal parameters, thus allowing a straightforward interpretation. In the same line, we have neglected in the present analysis any impurity-related intermediate state. A careful examination of some spectra (see Fig. 5) shows a reproducible bump around 2.545 eV which may be related to an exciton-neutral-donor bound-state one-photon resonance. Work is in progress to include the corresponding paths in the expression of $\chi^{(3)}$.

D. Configuration with the pump polarization parallel to the optical axis and that of the test and the signal perpendicular to it

The spectra of Fig. 7 are the first direct evidence of the possibility of reaching the Γ_1 biexciton and B_1 excitons in the $E \| \hat{c}$ configuration. They are quite similar in shape and the magnitude of their maxima are in the ratio 3 to 5. This can be used to evaluate the B_1-x_2 transition amplitude relative to the A_1-x_2 one as shown now. The two maxima occur about 3.5 meV below that of $\mathrm{Im}(\chi^{(3)})$ as shown in Figs. 6 and 10; therefore, the maximum conversion efficiency is in a region of low TPA, and it is legitimate to neglect the $(\kappa_2 I_p^0 l_a)$ terms in the denominator of Eq. (1b) to evaluate the signal intensity. The ratio of the maxima intensity in the two configurations simply is written

$$\frac{I_M^{\parallel}}{I_M^{\perp}} \simeq \left(\frac{(\kappa I_p(0) l_a)_{\parallel}}{(\kappa I_p(0) l_a)_{\perp}} \right)^2 .$$

The ratio of the pump intensities reduces to that of the transmission coefficients; that of the effective interaction lengths is deduced from the measured absorption coefficients ($l_a'' \simeq 23.5$ μm; $l_a^{\perp} \simeq 19.7$ μm. Finally, the modulus of the nonlinear coupling coefficients involves, besides the refractive index ($n_{\parallel}, n_{\perp}$), the modulus of the susceptibilities. We consider that the triply resonant terms have the dominant contribution; then the modulus of $\chi^{(3)}_{xxxx}$ and $\chi^{(3)}_{xzzx}$ are almost Lorentzian and do not depend on the Fano parameters (as long as the latter are larger than some units).

$$\frac{I_M^{\parallel}}{I_M^{\perp}} \simeq \left| \frac{\langle g|\mu_z|B_1\rangle\langle B_1|\mu_z|x_2\rangle}{\langle g|\mu_x|A_1\rangle\langle A_1|\mu_x|x_2\rangle} \right|^2 \left(\frac{D_A(W_{x_2})}{D_B(W_{x_2})} \right)^2 \left(\frac{n_{\perp}}{n_{\parallel}} \right)^2 \left(\frac{n_{\perp}+1}{n_{\parallel}+1} \right)^4 \left(\frac{l_a''}{l_a^{\perp}} \right)^2 .$$

By putting $D_A(W_{x_2}) \simeq 10$ meV and $D_B(W_{x_2}) \simeq 23$ meV one finds for $\rho = |\langle B_1|\mu_z|x_2\rangle|^2 / |\langle A_1|\mu_x|x_2\rangle|^2 \simeq 4$. The transition from the two excitons to the biexciton are thus of the same order of magnitude in CdS. That is to be put in relation with the fact that in the simplest model[29] the exciton-biexciton oscillator strength is the product of the ground state-exciton oscillator strength by a factor mainly involving the biexciton binding energy, and that in CdS $|\langle g|\mu_z|B_1\rangle|^2$ and $|\langle g|\mu_x|B_1\rangle|^2$ are roughly equal.

CONCLUSION

Through a simple method of active nonlinear spectroscopy we have investigated the Γ_1 biexciton in CuCl and CdS. We have shown that the propagation effects in nonlinear media have to be precisely accounted for to analyze correctly the experimental data. The high sensitivity of our method to the line shape of both $|\chi^{(3)}|$ and $\mathrm{Im}\chi^{(3)}$ has revealed the dissymmetry of the latter, which we have interpreted as arising from a Fano interference in a two-photon allowed transition. These two points have been used to analyze our experimental data and so to determine the main parameters of biexciton state in these compounds. They include the Fano q parameters as well as the exciton-biexciton oscillator strengths, all of which are summarized in Table I.

Among the problems which remain open to study in detail, one can mention the theory of the biexciton-continua coupling, which should explain the positive sign of the q parameters, and the investi-

TABLE I. Summary of the numerical values used in our fits. All energies are in eV; other quantities are dimensionless.

	CuCl	CdS
W_x	3.204	2.555 (A_1)
		2.568 (B_1)
Γ_x	0.5×10^{-3} (not sensitive)	2.0×10^{-4} (very sensitive)
W_{x_2}	6.372	5.096
Γ_{x_2}	0.5×10^{-3}	1.8×10^{-3}
q	15	6.0 (A_1)
$\frac{f_{xx_2}}{f_{gx}}$	1.0×10^{3}	2.3×10^{4} $x=A_1$
$\frac{f_{B_1x_2}}{f_{A_1x_2}}$		4

gation of the higher-order scatterings. Work is in progress on the two subjects in our laboratory.

ACKNOWLEDGMENTS

M. Batifol's expert skill has been intensively put to use in the experimental studies and Mrs. Bonnouvrier has devoted long hours in the programming work. They are both warmly thanked. We also thank Dr. Grün and Dr. Lévy from the Laboratoire de Spectroscopie du Corps Solide, l'Université de Strasbourg for providing us with high-purity CuCl samples and Dr. Planel from le Groupe de Physique des Solides de l'Ecole Normale Supérieure for providing us with high-purity CdS platelets. The work has benefited from a number of discussions with Dr. Bonneville and Dr. Oudar and the manuscript has been improved by their careful reading and suggestions.

APPENDIX: DIAGRAMMATIC REPRESENTATION OF THE THIRD-ORDER DENSITY MATRIX AND COMPUTATION OF THE THIRD-ORDER ELECTRIC DIPOLE

We follow here the formalism of Ref. 17. The left parts of the diagram (Fig. 12) represent the evolution of the ket and the right ones that of the bra. It is assumed that only the ground state $|g\rangle$ is initially populated; the interaction sequence is labeled so that transitions occur from the ground state to excited states in alphabetic order. Time

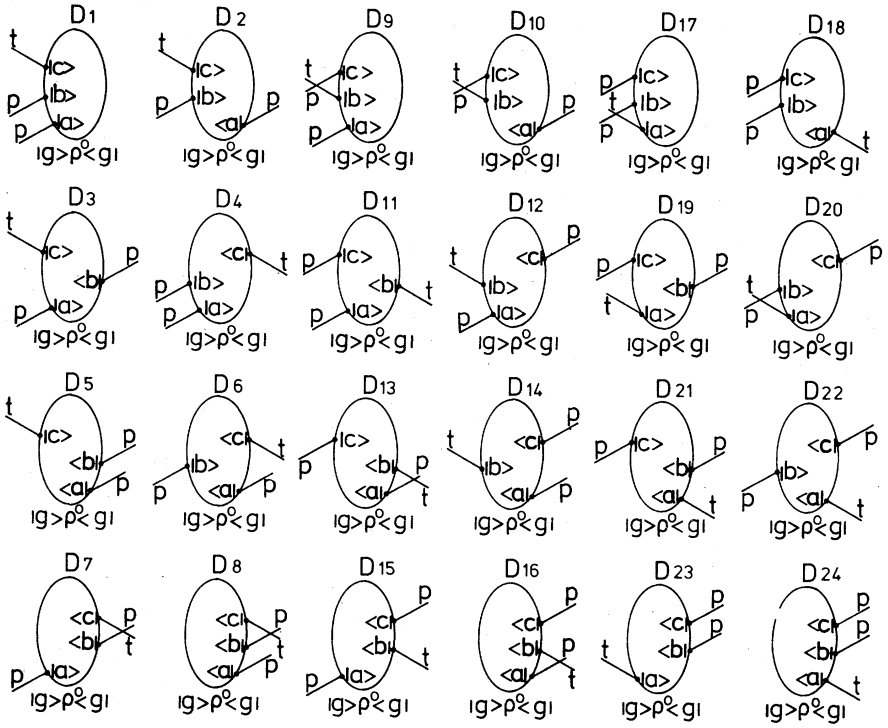

FIG. 12. Diagrammatic representation for the expression of the third-order density matrix. Each diagram corresponds to a series corresponding to the permutation of the different states. The right-side half of the ellipse corresponds to the evolution of the bra and the left-side half to that of the ket. Arrows pointing upward (downward) symbolize absorption (emission) transitions; p and t represent pump and test beam, respectively, and the degeneracy of the process reduces the number of nonequivalent diagrams from 48 to 24. Among those, 6 involve exciton-biexciton resonances; the other 18 decomposed into 1 triply resonant, 1 doubly resonant, 5 simply resonant, and 11 nonresonant terms.

increases upwards. At each vertex, the electromagnetic interaction is represented by a line pointing downwards for an absorption and upwards for an emission process. The practical rule for the sign of the contribution of each diagram is given here by $(-)^n$ where n is the number of interactions on the bra side of the time axis. Then, diagrams D_1 to D_8 correspond to the sequence absorption-absorption-emission (*aae*), diagrams D_9 to D_{17} correspond to the sequence (*aea*), and the diagrams D_{18} to D_{24} correspond to the sequence (*eaa*). Each diagram is to be considered as a series on the permutation of indices a, b, and c. When the third-order matrix $\chi^{(3)}$ is computed, one derives the third-order electric dipole $\mu^{(3)}$ through the relation

$$\mu^{(3)} = \mathrm{Tr}(\mu\rho^{(3)}) = \sum_{n,m} \rho^{(3)}_{nm}\mu_{mn}$$

with the notation $\Omega_{ig} = \omega_{ig} - i\Gamma_{ig}$; the "lexicographic" electric dipole is written as the following sum, where, so as not to be overhelmed by the notations, the tensorial indices and the sum on their permutations have been omitted:

$$\mu^{(3)} = \sum_{abc} \mu_I^{(3)},$$

$$\begin{aligned}
\mu_I^{(3)} \propto\ & + \frac{(\mu e_s^*)_{ec}(\mu e_t^*)_{cb}(\mu e_p)_{ba}(\mu e_p)_{ae}}{(\Omega_{ce}-\omega)(\Omega_{be}-2\omega)(\Omega_{ae}-\omega)} + \frac{(\mu e_s^*)_{ac}(\mu e_t^*)_{cb}(\mu e_p)_{be}(\mu e_p)_{ea}}{(\Omega_{ca}-\omega)(\Omega_{ba}-2\omega)(\Omega_{ae}^*+\omega)} \\
& - \frac{(\mu e_s^*)_{bc}(\mu e_t^*)_{ca}(\mu e_p)_{ae}(\mu e_p)_{eb}}{(\Omega_{bc}^*+\omega)(\Omega_{ba}^*+2\omega)(\Omega_{ae}-\omega)} - \frac{(\mu e_s^*)_{cb}(\mu e_p)_{ba}(\mu e_p)_{ae}(\mu e_t^*)_{ec}}{(\Omega_{bc}-\omega)(\Omega_{be}-2\omega)(\Omega_{ae}-\omega)} - \frac{(\mu e_s^*)_{bc}(\mu e_t^*)_{ce}(\mu e_p)_{ea}(\mu e_p)_{ab}}{(\Omega_{bc}^*+\omega)(\Omega_{be}^*+2\omega)(\Omega_{ae}^*+\omega)} \\
& - \frac{(\mu e_s^*)_{cb}(\mu e_t)_{be}(\mu e_p^*)_{ea}(\mu e_p)_{ac}}{(\Omega_{bc}-\omega)(\Omega_{ba}-2\omega)(\Omega_{ae}^*+\omega)} - \frac{(\mu e_s^*)_{ca}(\mu e_p)_{ae}(\mu e_p)_{eb}(\mu e_t^*)_{bc}}{(\Omega_{ac}-\omega)(\Omega_{ba}^*+2\omega)(\Omega_{ae}-\omega)} + \frac{(\mu e_s^*)_{ce}(\mu e_p)_{ea}(\mu e_p)_{ab}(\mu e_t^*)_{bc}}{(\Omega_{ce}^*+\omega)(\Omega_{be}^*+2\omega)(\Omega_{ae}^*+\omega)} \\
& + \frac{(\mu e_s^*)_{ec}(\mu e_p)_{cb}(\mu e_t^*)_{ba}(\mu e_p)_{ae}}{(\Omega_{ce}-\omega)(\Omega_{be})(\Omega_{ae}-\omega)} + \frac{(\mu e_s^*)_{ac}(\mu e_p)_{cb}(\mu e_t^*)_{be}(\mu e_p)_{ea}}{(\Omega_{ca}-\omega)(\Omega_{ba})(\Omega_{ae}^*+\omega)} + \frac{(\mu e_s^*)_{bc}(\mu e_p)_{ca}(\mu e_p)_{ae}(\mu e_t^*)_{eb}}{(\Omega_{bc}^*+\omega)(\Omega_{ab})(\Omega_{ae}-\omega)} \\
& - \frac{(\mu e_s^*)_{cb}(\mu e_t^*)_{ba}(\mu e_p)_{ae}(\mu e_p)_{ec}}{(\Omega_{bc}-\omega)(\Omega_{be})(\Omega_{ae}-\omega)} - \frac{(\mu e_s^*)_{bc}(\mu e_p)_{ce}(\mu e_p)_{ea}(\mu e_t^*)_{ab}}{(\Omega_{bc}^*+\omega)(\Omega_{be}^*)(\Omega_{ae}^*+\omega)} - \frac{(\mu e_s^*)_{cb}(\mu e_t^*)_{be}(\mu e_p)_{ea}(\mu e_p)_{ac}}{(\Omega_{bc}-\omega)(\Omega_{ba})(\Omega_{ae}^*+\omega)} \\
& + \frac{(\mu e_s^*)_{ca}(\mu e_p)_{ae}(\mu e_t^*)_{eb}(\mu e_p)_{bc}}{(\Omega_{ac}-\omega)(\Omega_{ab})(\Omega_{ae}-\omega)} + \frac{(\mu e_s^*)_{ce}(\mu e_p)_{ea}(\mu e_t^*)_{ab}(\mu e_p)_{bc}}{(\Omega_{ce}^*+\omega)(\Omega_{be}^*)(\Omega_{ae}^*+\omega)} + \frac{(\mu e_s^*)_{ec}(\mu e_p)_{cb}(\mu e_p)_{ba}(\mu e_t^*)_{ae}}{(\Omega_{ce}-\omega)(\Omega_{be})(\Omega_{ae}+\omega)} \\
& + \frac{(\mu e_s^*)_{ac}(\mu e_p)_{cb}(\mu e_p)_{be}(\mu e_t^*)_{ea}}{(\Omega_{ca}-\omega)(\Omega_{ba})(\Omega_{ae}^*-\omega)} + \frac{(\mu e_s^*)_{bc}(\mu e_p)_{ca}(\mu e_t^*)_{ae}(\mu e_p)_{eb}}{(\Omega_{bc}^*+\omega)(\Omega_{ab})(\Omega_{ae}+\omega)} - \frac{(\mu e_s^*)_{cb}(\mu e_p)_{ba}(\mu e_t^*)_{ae}(\mu e_p)_{ec}}{(\Omega_{bc}-\omega)(\Omega_{be})(\Omega_{ae}+\omega)} \\
& - \frac{(\mu e_s^*)_{bc}(\mu e_p)_{ce}(\mu e_t^*)_{ea}(\mu e_p)_{ab}}{(\Omega_{bc}^*+\omega)(\Omega_{be}^*)(\Omega_{ae}^*-\omega)} - \frac{(\mu e_s^*)_{cb}(\mu e_p)_{be}(\mu e_t^*)_{ea}(\mu e_p)_{ac}}{(\Omega_{bc}-\omega)(\Omega_{ba})(\Omega_{ae}^*-\omega)} + \frac{(\mu e_s^*)_{ca}(\mu e_t^*)_{ae}(\mu e_p)_{eb}(\mu e_p)_{bc}}{(\Omega_{ac}-\omega)(\Omega_{ab})(\Omega_{ae}+\omega)} \\
& + \frac{(\mu e_s^*)_{ce}(\mu e_t^*)_{ea}(\mu e_p)_{ab}(\mu e_p)_{bc}}{(\Omega_{ce}^*+\omega)(\Omega_{be}^*)(\Omega_{ae}^*-\omega)} .
\end{aligned}$$

---

*Laboratoire associé au CNRS (LA 250).

[1]N. Bloembergen, *Nonlinear Spectroscopy* (North-Holland, Amsterdam, 1977); D. S. Chemla and J. Jerphagnon in *Handbook on Semiconductors*, edited by M. Balkanski, (North-Holland, Amsterdam, 1980), Vol. 2, Chap. 9.

[2]P. D. Maker and R. W. Terhune, Phys. Rev. 137A, 801 (1965).

[3](a) A. Maruani, J. L. Oudar, E. Batifol, and D. S. Chemla, Phys. Rev. Lett. 41, 1372 (1978); (b) J. L. Oudar, A. Maruani, E. Batifol, and D. S. Chemla, J. Opt. Soc. Am. 68, 11 (1978).

[4]E. Hanamura and H. Haug, Phys. Rep. 33, 4 (1977).

[5]R. Lévy and B. Hönerlage, to be published in the proceedings of the 1980 Conference Condensed Matter Division (European Physical Society Antwerpen, 1980).

[6](a) R. Lévy, B. Hönerlage, and J. B. Grün, Phys. Rev. B 19, 2326 (1979); (b) M. Mita and N. Nagasawa, Opt. Commun. 24, 435 (1978); (c) M. Ojima, T. Kushida, S. Shionoya, Y. Tanaka, and Y. Oka, J. Phys. Soc. Jpn. 45, 3 (1978); (d) M. Ojima, Y. Yoka, T. Kushida, and S. Shionoya, Solid State Commun. 28, 845 (1977); (e) B. Hönerlage, Vu Duy Phach, and J. B. Grün, Phys. Status Solidi B 88, 545 (1978); (f) N. Nagasawa, T. Mita, and M. Ueta, J. Phys. Soc. Jpn. 41, 929 (1976).

[7](a) J. M. Hvam, Solid State Commun. 26, 373 (1978); (b) I. Rückmann, J. Puls, and J. Voigt, Phys. Status Solidi B 87, K111 (1978); A. Kuroiwa, H. Saito, and S. Shionoya, Solid State Commun. 18, 1107 (1976); (c) Y. Nozue, T. Itoh, and M. Ueta, J. Phys. Soc. Jpn. 44, 1305 (1978); H. Schrey, V. G. Lyssenko, and C. Klingshirn, Solid State Commun. 17, 299 (1979); T. Itoh, Y. Nozue, and M. Ueta, J. Phys. Soc. Jpn. 40, 6 (1976); (d) R. W. Svorec and L. L. Chase, Solid State Commun. 17, 803 (1975); (e) R. Planel and

C. Benoît à la Guillaume, Phys. Rev. B 15, 1192 (1977); F. Henneberger and J. Voigt, Phys. Status Solidi B 79, K81 (1977); (f) H. Schrey, V. G. Lyssenko, and C. Klingshirn, Solid State Commun. 32, 897 (1979).

[8]D. S. Chemla, A. Maruani, and E. Batifol, Phys. Rev. Lett. 42, 1075 (1979).

[9]A. Maruani, IEEE J. Quantum Electron. 16, 558 (1980). As a result of a circular permutation between Figs. 2–6 and captions 2 to 6, caption 2 goes with Fig. 3, caption 3 with Fig. 4, ··· until caption 6 with Fig. 2.

[10]J. Armstrong, N. Bloembergen, J. Ducuing, and P. S. Pershan, Phys. Rev. 127, 1918 (1962).

[11]N. Bloembergen, *Nonlinear Optics* (Benjamin, New York, 1965).

[12]P. N. Butcher, *Nonlinear Optical Phenomena*, Bulletin 2000 (Ohio State University, Columbus, 1965); for a review of the theory of third-order susceptibilities see C. Flytzanis in *Quantum Electronics: A* Treatise, edited by H. Rabin and C. L. Tang (Academic, New York, 1975), Vol. I, Part A.

[13]H. Eecher, IEEE J. Quantum Electron. 11 4 (1975).

[14]Sh.M. Kogan, Zh. Eksp. Teor. Fiz. 43, 304 (1962) [Sov. Phys.—JETP 16, 217 (1962)]; M. Asdente, M. C. Pascucci, A. M. Ricca, and P. Venturini, Solid State Commun. 15, 1551 (1974).

[15]H. Mahr in Quantum Electronics: A Treatise (Academic, New York, 1975), Vol. I, Part A, p. 285

[16]F. Bassani, J. J. Forney, and A. Quattropani, Phys. Status Solidi B 65, 591 (1974); E. Doni, R. Girlanda, and G. Pastori Parravicini, Phys. Status Solidi B 88, 773 (1978).

[17]S. Y. Yee, T. K. Gustavfson, S. A. J. Druet, and J. P. Taran, Opt. Commun. 23, 1 (1977).

[18]S. A. J. Druet, J. P. Taran, and Ch. J. Bordé, J. Phys. (Paris) 40, 819 (1979).

[19]E. Hanamura and T. Takagahara, J. Phys. Soc. Jpn. 42, 410 (1979).

[20]N. Bloembergen, H. Lotem, and R. T. Lynch, Indian J. Pure Appl. Phys. 16, 151 (1978).

[21]I. Shoshan, N. N. Danon, and U. Oppenheim, J. Appl. Phys. 48, 4495 (1977).

[22]B. Hönerlage, A. Bivas, and Vu Duy Phach, Phys. Rev. Lett. 41, 49 (1978).

[23]U. Fano, Phys. Rev. 124, 1866 (1961); J. P. Connerade, Proc. R. Soc. London xx, 361–374 (1978); A. Nitzan, Mol. Phys. 27, 1 (1974); 27, 65 (1974); see also *Etats Atomiques et Moléculaires Couplés à un continuum; Atomes et Molecules Hautement Excites*, Proceedings of the International Meeting No. 273 of the CNRS, edited by S. Feneuille and J. C. Lehmann (CNRS, Paris, 1977).

[24]J. A. Armstrong and J. J. Wynne, Phys. Rev. Lett. 33, 1183 (1974).

[25]M. Ueta and N. Nagasawa in *Physics of Highly Excited States in Solids*, edited by M. Ueta and Y. Nishina (Springer, Berlin, 1976).

[26]Vu Duy Phach, A. Bivas, B. Hönerlage, and J. B. Grün, Phys. Status Solidi B 84, 731 (1977).

[27]K. Arya and A. R. Hassan, Solid State Commun. 21, 301 (1977).

[28]W. Eckardt and M. I. Sheboul, Phys. Status Solidi B 74, 523 (1976).

[29]E. J. Rashba in *Excitons at High Density*, edited by H. Haken and S. Nikitine (Springer, Berlin, 1975); E. Hanamura, Solid State Commun. 12, 951 (1973).

[30]A. Maruani, D. S. Chemla, and E. Batifol, Solid State Commun. 33, 7 (1980).

[31]J. Jackel and H. Mahr, Phys. Rev. B 17, 3387 (1978).

[32]W. C. Tait, Phys. Rev. B 5, 648 (1972).

[33]B. F. Levine, R. C. Miller, and W. A. Nordland, Jr., Phys. Rev. B 12, 4512 (1975).

[34]J. J. Hopfield, Phys. Rev. 182, 3 (1969).

[35]P. Yu and S. Evangelisti, Phys. Rev. Lett. 42, 1642 (1979); I. Broser and M. Rosenzwaig, Phys. Status Solidi 90, 77 (1978).

[36]C. Flytzanis and N. Bloembergen in *Progress in Quantum Electronics*, edited by Sanders and Stenholm (Pergamon, New York, 1976), Vol. 4, p. 3.